Accepted for publication in Small (Wiley)
Published online: May 19, 2017 (DOI:10.1002/smll.201700384)

Healing effect of controlled anti-electromigration on conventional and high-T_c superconducting nanowires

Xavier D. A. Baumans,[1] Joseph Lombardo,[1] Jérémy Brisbois,[1] Gorky Shaw,[1] Vyacheslav S. Zharinov,[2] Ge He,[3] Heshan Yu,[4] Jie Yuan,[3] Beiyi Zhu,[3] Kui Jin,[3] Roman B. G. Kramer,[5, 6] Joris Van de Vondel,[2] and Alejandro V. Silhanek[1]

[1]*Experimental Physics of Nanostructured Materials, Q-MAT, CESAM, Université de Liège, B-4000 Sart Tilman, Belgium**
[2]*INPAC – Institute for Nanoscale Physics and Chemistry, Nanoscale Superconductivity and Magnetism Group, K.U.Leuven, B–3001 Leuven, Belgium*
[3]*Beijing National Laboratory for Condensed Matter Physics, Institute of Physics, Chinese Academy of Sciences, Beijing 100190, China*
[4] *Beijing National Laboratory for Condensed Matter Physics, Institute of Physics, Chinese Academy of Sciences, Beijing 100190, China*
[5]*Université Grenoble Alpes, Institut NEEL, F-38000 Grenoble, France*
[6]*CNRS, Institut NEEL, F-38000 Grenoble, France*

The electromigration process has the potential capability to move atoms one by one when properly controlled. It is therefore an appealing tool to tune the cross section of monoatomic compounds with ultimate resolution or, in the case of polyatomic compounds, to change the stoichiometry with the same atomic precision. We demonstrate that a combination of electromigration and anti-electromigration can be used to reversibly displace atoms with a high degree of control. This enables a fine adjustment of the superconducting properties of Al weak links, whereas in Nb the diffusion of atoms leads to a more irreversible process. In a superconductor with a complex unit cell ($La_{2-x}Ce_xCuO_4$), the electromigration process acts selectively on the oxygen atoms with no apparent modification of the structure. This allows us to adjust the doping of this compound and switch from a superconducting behaviour to an insulating state in a nearly reversible fashion. We discuss the conditions needed to replace feedback controlled electromigration by a simpler technique of electropulsing. These findings have a direct practical application as a method to explore the dependence of the characteristic parameters on the exact oxygen content and pave the way towards a reversible control of local properties of nanowires.

Introduction

The displacement of atoms caused by high electric current densities was already identified in the late 1960s as a major failure problem of narrow Al interconnects in integrated circuits and other electronic devices[1–4]. The negative perception of this phenomena, known as electromigration (EM), has progressively changed during the last decades, as the scientific community first understood the physical mechanisms involved in the process and then learnt to master it[5–7].

Examples illustrating the benefits of controlling the EM process include the creation of few nanometer gaps between two Au pads[8–12] with the aim to electrically address single molecules[13–15], the electrical sculping of nanowires to obtain atomic point contacts[16–18], metal purification and separation of atoms in binary alloys due to the mass selectivity of the process[19], current-induced crystallization[20], and cleaning of graphene layers[21].

Arguably, one of the most appealing aspects of EM is the reversibility of the mechanism. Indeed, it has been shown that nanogaps, once created, can be closed by using voltage spikes[16,22] while refilling of previously generated voids has been demonstrated in metals such as Al and Pd-Pt[23–25] by simply reversing the polarity of the dc current.

In this work, we introduce controlled EM as a powerful tool to explore superconducting nanoconstrictions. We show that this technique successfully works for Al, Nb, and $La_{2-x}Ce_xCuO_4$ (LCCO), three dissimilar superconductors. The reversed migration, here coined as anti-electromigration (anti-EM), allows us to heal the modifications previously produced by EM and partially recover the original superconducting properties of the nanoconstriction. In addition, we establish the possibility to finely tune the resistance of such a nanowire by using successive runs of EM/anti-EM. A similar effect is observed in non-conventional (cuprate-based compounds) superconducting microbridges, whereas it works only partially in Nb. In addition, we investigate an alternative controlled EM procedure consisting of electro-pulsing. This method is more accurate in terms of reaching the aimed resistance, is faster than continuously monitoring EM, and much simpler to implement without the need of complex feedback loop controllers. The presented effects could be used as an appealing and interesting alterna-

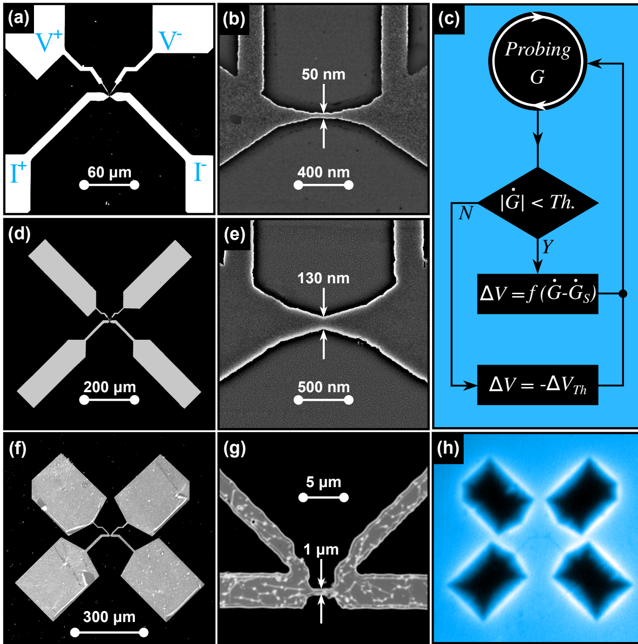

FIG. 1: **Sample layout and flowchart of the control feedback loop.** (a-b) Scanning electron microscopy images of the investigated Al samples obtained for two different magnifications. (c) Schematic diagram of the algorithm used to achieve controlled electromigration. (d-e) Scanning electron microscopy images of the investigated Nb samples obtained for two different magnifications. (f-g) Optical microscopy images of the investigated LCCO samples at two different magnifications. (h) Magneto-optical image of a LCCO sample obtained at $H = 1$ mT and $T = 3.6$ K, illustrating the smooth penetration of magnetic flux.

tive for manipulating the superconducting properties of nanowires. Particularly relevant is the possibility to reversibly change the stoichiometry of high temperature superconductors without the need to fabricate different samples.

Results and discussion

The investigation has been conducted on three different superconducting compounds, Al (T_c=1.39 K), Nb (T_c=8.7 K) and $La_{2-x}Ce_xCuO_4$ (LCCO, T_c=26.1 K), covering a wide range of superconducting parameters (see Experimental Section). All samples consist of a transport bridge with a central constricted section, as it is shown in Figure 1 for Al [a,b], Nb [d,e] and LCCO [f-h]. The sudden reduction of the width at the centre of the bridge is intended to increase the probability to migrate atoms in its vicinity. This is a natural consequence from the fact that electromigration is driven by temperature T and current density J as described by Black's formula for the mean lifetime of the nanowire[4] τ given by,

$$\tau = wt\frac{\exp(\frac{U}{k_B T})}{J^2}, \qquad (1)$$

where U is the activation energy needed to displace an atom, while w and t correspond to the width and thickness of the wire, respectively.

Figure 1c represents a simplified diagram of the main algorithm used to control EM. For all measurements presented in this work, the electromigration has been carried out in a cryogenic environment with bath temperature T_B just above the critical temperature of the concerned superconductor. More details about sample fabrication and EM software are given in the experimental section.

Electromigration of Al nanoconstrictions

The polycrystalline structure and the associated grain boundaries have been recognized as essential ingredients for explaining electromigration. This has been clearly demonstrated by the fact that eletromigrating Al single crystals is considerably more difficult than EM polycrystalline Al[5]. While electromigration of relatively large (several micrometers) Al bridges has been reported in Ref. 4,23,24, little is known about electromigration in nanoscale Al wires and constrictions. Figure 2a shows a typical evolution of the sample resistance, R, as a function of the applied current, I, during a controlled electromigration process of Al. The nearly parabolic increase of R with increasing I arises from the local increase of temperature due to Joule heating. Indeed, on the one hand, the sample resistance is given by $R(T) = R(T_B)(1+\alpha(T-T_B))$ with α the thermal coefficient. On the other hand, the temperature at the constriction results from the balance of input power, $R(T)I^2$, and heat removal $h(T-T_B)$, which gives $R(I) \approx R(T_B)(1 + \alpha R(T_B)I^2/h + \mathcal{O}(I^4))$, where h characterizes the heat removal mechanism which combines heat transfer to the substrate, the thermal conduction towards the leads, K, and the convection with the surrounding medium (liquid He in the present case). For Al, this part of the $R(T)$ curve is fully reversible and does not lead to mass transport. Electromigration takes place in the region where the current through the constriction diminishes while the resistance increases. This regime with negative dR/dI is irreversible and leads to permanent damage of the nanoconstriction as evidenced by the scanning electron microscopy (SEM) image shown in the inset of Figure 2e. A careful look at this SEM image reveals two important features. First, the void does not take place exactly at the isthmus of the constriction. This is a consequence of the fact that EM occurs mainly along grain boundaries and it is not solely ruled by the point of highest current density. Second, the section of the constriction on the right hand side of the void does not exhibit the same granularity as the virgin sample. This observation lead us to believe that a change of crys-

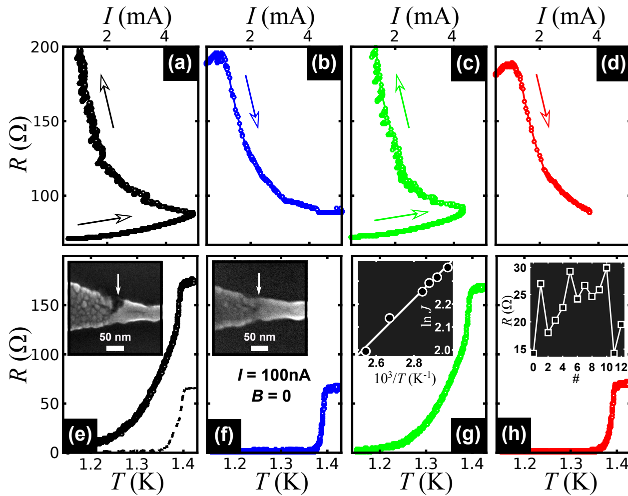

FIG. 2: **Anti-electromigration in Al nanowires.** (a-d) Electromigration curves showing the evolution of resistance as a function of current. Panels (e-h) show the $R(T)$ curves obtained after each EM ((e) and (g)) and anti-EM ((f) and (h)). Insets in (e) and (f) are scanning electron micrograph evidencing the creation and healing of a void at the constriction of the nanowire. The dashed line in panel (e) shows the response of the virgin sample. The inset in panel (g) shows the linear relation between $\ln J$ and T^{-1}, for the (T, J) points corresponding to the maximum current density and local temperature. Inset in (h) represents the chronology of the resistance obtained during 12 successive runs of EM/anti-EM on the same nanowire at $TB = 1.5$ K.

talline structure happened during the EM process. This is in agreement with previous investigations[20].

Notice that EM starts at $I \sim 5$ mA, corresponding to a maximum current density of 400 MA/cm^2 at the narrowest point along the bridge. This value is obtained with a constant rate of decreasing conductance dG/dt. Based on Equation (1), we can conclude that the lower the T, the higher the J needed for achieving the point where dR/dI changes sign. This is confirmed by the linear relation between $\ln(J)$ and $1/T$ as shown in the inset of Figure 2g. Here the (T, J) points correspond to the maximum current density and the local temperature at this current value. The slope of this graph provides an activation energy $U \sim 0.3$ eV which is significantly smaller than the 1.4 eV for the lattice self-diffusion of Al[26,27] but not far from the 0.48 eV reported by Black[4] in polycrystalline samples. This is not surprising considering that both, grain boundary and surface diffusion, are the predominant transport mechanisms with a reduction factor depending on the size of the grains[28]. When constructing the plot shown in the inset of Figure 2g, care must be applied to calculate the temperature T at the constriction, which can largely exceed the bath temperature T_B. Numerical simulations of the heat transfer equation for our particular geometry and cryogenic environment[18] showed that the electromigration starts when the local temperature at the constriction is about $T \sim 200$ K for $T_B = 1.5$ K. Similar values can be obtained using the analytic expression for the temperature of the current-heated nanowire given in Ref. 29. A rougher albeit simpler estimate of the temperature along the parabolic segment of the $R(I)$ curve can be obtained from the expression,

$$T = T_{\rm B} + \alpha^{-1}\frac{R(T) - R(T_{\rm B})}{R(T_{\rm B})}, \qquad (2)$$

This formula is valid as long as a linear temperature dependence of the resistance and no change of the structure of the system is observed. Application of Equation (2) to the particular case of the electromigration curve shown in Figure 2a, for which $\alpha = 0.80 \times 10^{-3}$ K^{-1} ($RRR = 1.85$), suggests that EM already starts at 100 K. Equation (2) implicitly assumes that the temperature rise is rather uniform between the voltage contacts. This is justified by the fact that the width of the spatial temperature distribution, so called thermal healing length[30], $\delta = \sqrt{Kt/h} \sim 1\mu$m for granular Al[31], is larger than the separation between the constriction and the voltage contacts. Still, the temperature values obtained from Equation (2) represent an underestimation by about 30% of the temperature of the hottest spot along the nanowire[32,33].

After the first EM shown in Figure 2a, the normal state resistance has increased by a factor of 3. Only based on transport measurements it is highly non trivial to draw any reliable conclusion concerning the effective cross section reduction of the nanoconstriction. Indeed, depending on the chosen parameters driving the electromigration, voids can develop either at the center of the bridge or along its perimeter[34]. To that end, it is essential to carry out direct imaging of the induced damage as shown in the inset of Figure 2e. The $R(T)$ curve obtained in zero field condition and with an applied current $I = 100$ nA, much smaller than the one needed to initiate the EM, reveals a superconducting transition substantially broader than the one corresponding to the virgin sample shown with a dotted line in Figure 2e. This has been interpreted in terms of thermally activated phase slips phenomena[18] where $R(T) = R_0 \exp(-\Delta F/k_{\rm B}T)$, with $\Delta F \propto w$ the activation energy associated to the creation of a phase slip excitation. As w decreases, so does ΔF and consequently the rate of phase slips and the associated dissipation increase. It is also worth noting that the narrowing of the constriction does not seem to produce a change in the critical temperature as could be expected from previous reports[35]. This effect results from the fact that the voltage contacts are 500 nm apart from the constriction and therefore capture also the superconducting transition of the leads which remains unchanged after EM. Further electromigrating the sample accentuates the narrowing of the constriction and consequently increases the rate of phase slips and broadens the superconducting transition even more.

The most interesting result is summarized in the second column of Figure 2. Panel (b) of Figure 2 shows that

by inverting the direction of the electromigrating current, it is possible to anti-electromigrate, i.e. to reduce the resistance as current increases. A similar effect has been reported for Au and Pd-Pt nanowires[25]. As shown in the inset of Figure 2f corresponding to the SEM image after anti-EM, the void has been refilled with material, naturally explaining the observed decrease in resistance. It is important to remark that all SEM images have been acquired *ex-situ*, which requires removing the sample from the cryostat at expenses of risking an electrostatically induced damage. Figure 2f confirms that a sharp superconducting transition, very close to the initial virgin sample (dotted line in Figure 2e), is recovered after anti-EM. An extra sequence of EM (panels (c) and (g)) followed by anti-EM (panel (d) and (h)) unambiguously shows the reversibility of this process in Al samples.

Further evidence of the controllability of the normal state resistance by alternating EM and anti-EM is shown in the inset of Figure 2h. Here, each resistance value achieved by EM differs from the targeted value by less than 0.25 Ω, demonstrating the fine tuning capability of the process. Considering that this process is realized in the very same sample, being reversible and with high level of control, it can be considered as an appealing approach to study the evolution of the physical properties of nanoconstrictions of different conducting materials. The question now arises as to whether Al is a particularly malleable material permitting this manipulation and if the observed behaviour can be generalized to other compounds. In the next sections we will discuss the cases of Nb and LCCO and show that there are some particularities in the electromigration process which are unique to each material.

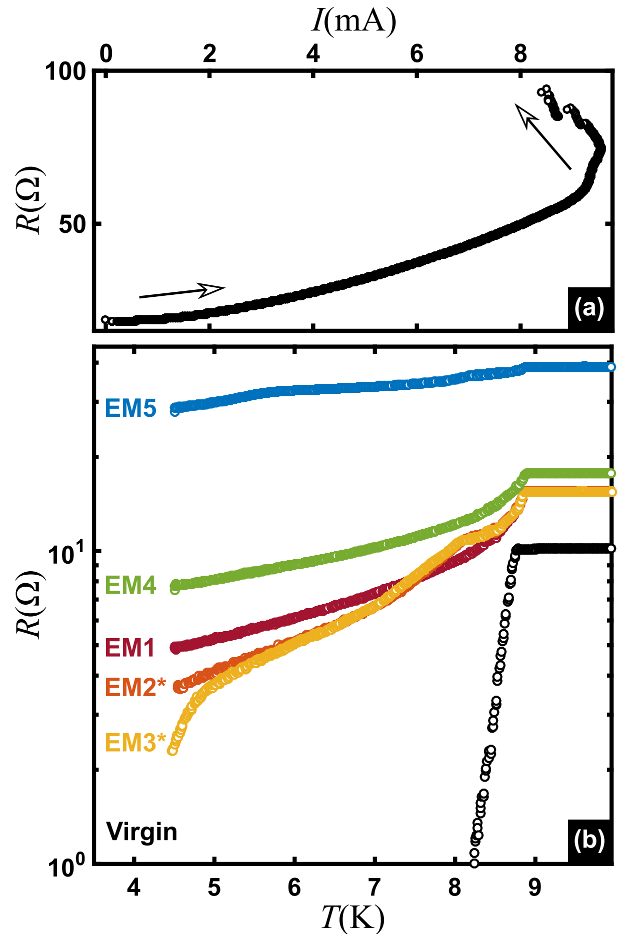

FIG. 3: **Electromigration in Nb nanoconstrictions.** (a) Evolution of resistance as a function of current during an electromigration process. (b) Resistance vs temperature obtained at low drives (1 μA) obtained after a series of EM/anti-EM processes. Numbers indicate the chronological order. Asterisks denote anti-electromigration runs.

Electromigration of Nb nanoconstrictions

The electromigration of Nb has not received much attention so far. The early works of Serruys[36,37] deal with mm size samples and focus on the displacement of iron, cobalt and chromium immersed in Nb as measured by a radioactive tracer method. The electromigration force is given by $\mathbf{F} = Z^* e\mathbf{E}$, where e is the electron charge, $\mathbf{E}$ is the electric field, and Z^* is the effective valence of the carriers combining the effect of electron wind and direct electric force on the ions[28]. As recognized by Gupta et al.[38], the electron-wind force, responsible for electromigration, depends on an integral over the Fermi surface which is rather complicated and essentially hole-like in Nb, i.e. $Z^* > 0$. This is in contrast to Al for which $Z^* < 0$.

In Figure 3a we show the evolution of the resistance of a Nb constriction during the EM process. The general aspect of the curve resembles the response of Al nanoconstrictions, but a more careful analysis permits us to identify two important differences. First, the initial increase of resistance is, unlike for Al, irreversible and leading to changes in the superconducting properties of the constriction. Second, the current at which dR/dI changes polarity (threshold of severe electromigration) is not sharply defined but rather a smooth transition is observed. We estimate at about 140 MA/cm^2 the threshold current density needed to start severe electromigration at a bath temperature of 10 K. From the normal state resistance we obtain a resistivity $\rho \sim 9$ $\mu\Omega$cm for the Nb films at 10 K and a RRR=3.65 corresponding to $\alpha = 9.08 \times 10^{-3}$ K^{-1}. From these parameters and using Equation (2) we can deduce, assuming minor changes in the structure, that the temperature at the maximum applied current is $T \sim 760$ K. It should also be mentioned that the transport measurements in Nb have been performed in a chamber with a He pressure of 2 mbar with most of the heat removal through the substrate.

Figure 3b shows $R(T)$ curves obtained at low drives (1 μA) after different electromigration histories. As for Al, the onset of the superconducting transition does not change after electromigration, indicating that this crite-

rion denotes the transition in the electrodes rather than at the constriction. The first electromigration (EM1), obtained after applying 8.4 mA, gives rise to an increase of the normal state resistance as well as a much broader transition than the virgin sample. This effect is very similar to the Al constrictions and can thus be attributed to the enhanced effects of thermal fluctuations. Interestingly, even though this EM has been carried out at a current smaller than the one corresponding to the transition to the $dR/dI < 0$ regime, a clear change in the material properties is still observed. SEM images acquired at this stage of the process show no hint of structural damage. Starting from this point, two consecutive attempts of anti-EM (EM2 and EM3) lead to a rather weak recuperation of the superconducting state, but producing no noticeable change in the normal state resistance. Changing the polarity of electromigration back into the initial condition and always dwelling within the regime where $dR/dI > 0$, we are able to further increase the normal state resistance and widen the superconducting transition as shown in EM4. The curve EM5 results from a severe electromigration in the $dR/dI < 0$ regime.

In general, we confirm that forward electromigration in Nb seems to operate correctly whereas anti-EM produces very weak recovery of the superconducting properties. In other words, there is little influence of the current polarity into the final resistive state. This is in striking contrast to what is observed in Al. In order to understand this behavior it is necessary to recall that Nb is not in a pure state but it contains interstitial solute atoms of oxygen. De Sorbo[39] has shown that for each 1% at. of O in Nb, the superconducting transition T_c decreases by 0.93 K and the normal state resistivity increases by 5.2 $\mu\Omega$ cm. The fact that the critical temperature of our samples lies about 0.4 K below the expected value for pure Nb can be interpreted as an indication of O diffused into the structure. In Ref. 40 it was shown that O diffusion in Nb becomes important above 400 K whereas at 300 K the diffusion of O in defect-free Nb is only of 0.1 nm in three days. Considering that our rough estimate of the sample temperature at the point of starting the electromigration lies largely above 400 K and that the chamber of the cryostat is not in ultra high vacuum conditions, it is plausible that O diffusion takes place during the EM. In addition, the strain along grain boundaries and defects is known to yield an enhanced O concentration and diffusion[41,42]. Based on this information and the presented experimental results, we envisage a scenario where EM in Nb occurs in two steps. At low currents, O atoms are subjected to migration thus leading to clear changes in the superconducting properties and the normal state resistance. In this regime, no noticeable changes of the structure are expected. At large bias currents ($dR/dI < 0$), Nb atoms can be displaced and a more conventional electromigration takes place.

Considering that a strong directional bond between Nb and O gives rise to large binding energies above 5 eV[43,44] it would be interesting to verify our hypothesis in an alternative system where O atoms were more susceptible to be displaced by an electron current. To that end, in the next section we focus our attention on a copper oxide superconducting compound.

Electromigration of LCCO microconstrictions

A pioneer investigation of electromigration of oxygen in the prototypical high critical temperature superconductor $YBa_2Cu_3O_{7-\delta}$ at 200 °C has been reported in Ref. 45. Later on, Moeckly and co-workers[46–48] have addressed the electromigration in micron size bridges of this material at room temperature. These authors reported an improvement of the normal and superconductive properties of the microbridge, raising J_c, and lowering the normal state resistivity by up to 30% for currents below a threshold bias of about 5 MA/cm^2. Above this threshold the transport properties were shown to rapidly degrade. The detrimental effects were attributed to the electromigration of basal-plane oxygen and the resultant formation of inhomogeneous oxygen deficient and disordered distributions giving rise to filamentary superconducting regions of nanometer scale within a nonsuperconducting background. Interestingly, the authors also reported that moderately damaged structures may be effectively restored by subsequent application of a large dc current with the opposite polarity. In other words, similarly to the case described for Nb, the effect of EM is not to produce a morphological change but to create oxygen deficient regions.

We have extended these early investigations to a sister compound, $La_{2-x}Ce_xCuO_4$. In our case, the EM is carried out at low temperatures, allowing us to access a regime of rather cold electromigration. As shown in Figure 4a, the electromigration process resembles that of Nb, with an initial parabolic shape of the $R(I)$ characteristic followed by a smooth transition to the region where $dR/dI < 0$. Along the region where $dR/dI > 0$, the response is reversible as in Al. In the region of negative slope the response is irreversible although it generates no visible damage to the structure. This is shown by comparing the SEM images corresponding to the virgin sample in Figure 5a to that of the same sample after electromigration in the negative slope regime (see Figure 5b). If, however, very high current densities are applied, a clear imprint of the damage caused in the structure is observed, as indicated by the arrow in Figure 5c after applying 80 MA/cm^2. We argue that at relatively low current densities, only oxygen atoms are displaced by the electron wind, whereas at sufficiently high current densities heavier atoms are able to migrate within the unit cell. In addition, in our polycrystalline LCCO sample, highly strained grain-boundary regions may contain excess O vacancies as reported for YBCO[49], and can further influence the change of local oxygen doping via electromigration.

Evidence of the irreversible response obtained after

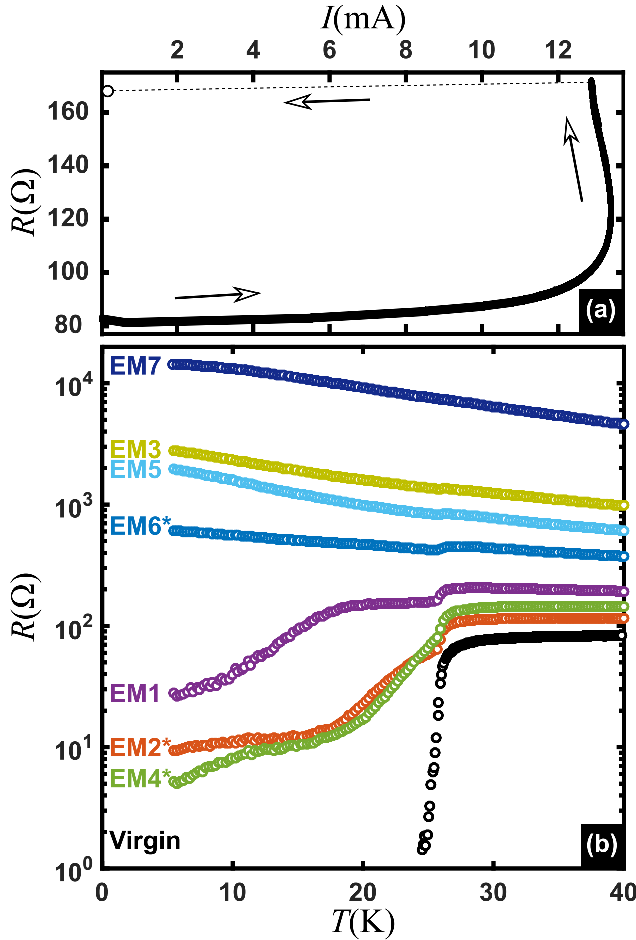

FIG. 4: **Electromigration-healing sequences in LCCO microwires.** (a) typical $R(I)$ response during an electromigration process in LCCO at a bath temperature of 30 K. (b) Resistance versus temperature characteristics of a LCCO microbridge after successive electromigrations. Numbers indicate the chronological order. Asterisks denote anti-electromigration runs.

electromigration with weak currents is shown in Figure 4b where the $R(T)$ characteristics obtained with a bias current $I = 1$ μA are shown after successive electromigrations. The virgin sample, i.e. before electromigration, exhibits a superconducting transition at about 26 K. After the first electromigration process (EM1) the normal state resistance has been increased by 110 Ω and the superconducting transition defined at 50% criterion, has diminished by a factor of 1.7. This change can be partially healed by reversing the current direction (EM2). If the resistance of the constriction is brought above 350 Ω the superconducting transition is no longer present in the range of temperatures here investigated. Instead, an increase of resistance with decreasing T, characteristic of an insulating state, is observed. Interestingly, the superconducting state can still be recovered by anti-EM (see curve EM4).

To our knowledge, this is the first evidence of current-driven superconductor-insulator transition (SIT) in LCCO films. In order to dig into the possible scenarios describing the mechanism behind this phenomena, let us first remind some important facts concerning these materials. The electron-doped LCCO is in the so called T' structural phase, while the hole-doped counterpart $(La,Sr)_2CuO_4$ (LSCO) has a T-type structure. In the T-phase, one Cu atom and six oxygen atoms form an octahedron, whereas in the T'-phase the two apical oxygens are removed or moved to the rare-earth blocks (see Fig1 in Ref. 50). The YBCO has a T* structure, where only one apical oxygen is detached from the octahedron. Interestingly, a T'-to-T structure transition with tuning pressure was observed in $(Pr,Ce)_2CuO_4$, accompanied with a superconductor-insulator transition[51] which might suggest that large current densities can play the same role as pressure on oxygen migration. Another plausible interpretation of the reversible SIT is that oxygen is pushed away from the original position under high current density, resulting in a gradual distortion of the lattice along the bridge. This is consistent with the increase of the residual resistivity with increasing oxygen content as reported in Ref. 50. Similar electrically driven redox reaction and the associated structural change has been observed in Ce oxides[52]. We should also mention that the reversible change of the bridge resistance could be associated to the resistive switching observed in transition metal oxides, for which the generation of oxygen vacancies has been identified as one of the possible mechanisms. Clearly, futher investigations are needed to discern which among the above listed phenomena, is the dominant one.

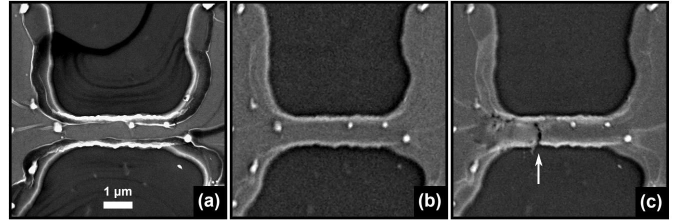

FIG. 5: **Structural characterization of electromigration in LCCO microbridge.** (a) Scanning electron micrograph of virgin high-T_c microbridge. (b) Micrograph of the same bridge as in (a), taken after electromigration (EM2). (c) Very last state of the bridge taken after having applied high voltage to increase resistance until measuring current values characteristic of tunnelling.

It is worth noting that the transition point where dR/dI changes sign takes place at a critical current density of 13 MA/cm^2 when done at a bath temperature of 50 K. We estimate a resistivity $\rho \sim 150$ $\mu\Omega$cm for the LCCO films at 50 K and a RRR=5.3 corresponding to $\alpha = 17.3 \times 10^{-3}$ K^{-1}. From these parameters and using Equation (2) we can estimate that the maximum temperature during the electromigration is $T \sim 70$ K.

Finally, it is interesting to consider the possibility that the critical current density of a superconductor can ex-

ceed the density of current needed for EM. This may be achieved in high critical temperature superconductors like YBCO where $J_c \sim 3$ MA/cm^2 at 77 K and $J_c \sim 30$ MA/cm^2 at 10 K. Since these values of current densities lie above the current needed to migrate oxygen atoms, in case the dissipative regime of the superconductor is achieved, EM takes place and the properties of the material change irreversibly. Notice as well that if the stoichiometry of the compound is detuned by current, also the carrier density should be affected. We are not aware of studies addressing these issues.

Electropulsing

As we have pointed out above, severe electromigration starts at the point where dR/dI diverges, i.e. where a transition from $dR/dI > 0$ to $dR/dI < 0$ takes place. It is important to emphasize that this transition results from the reaction to the feedback signal and therefore its degree of abruptness reflects the speed with which this feedback control needs to operate. In other words, more pronounced is the curvature of the $R(I)$ at the transition, faster the feedback loop needs to react. The electromigrations performed in Nb (Figure 3a) and LCCO (Figure 4a) exhibit a rather smooth transition suggesting that the EM process corresponds to a progressive damage instead of an explosive phenomenon. This finding encouraged us to propose the simpler method of electropulsing as an alternative to achieve controlled electromigration, without the need of costly and complex feedback loops. This approach consists in applying voltage pulses of magnitude similar to that needed to reach the critical current density of the virgin structure during a short period of time. The results obtained through this technique are summarized in Figure 6.

The main panel of Figure 6 shows the evolution of the final resistance of the constriction after a series of voltage pulses of amplitude 15 V and duration 1 s. The initial resistance of the sample (300 Ω) was first increased up to 1100 Ω and subsequently reduced to its initial value by applying pulses of negative polarity. A similar procedure applied to Nb (see inset of Figure 6) shows an increase of the initial resistance by a factor of 7. Pulses of negative polarity in Nb lead to very weak healing effects (not shown), in agreement with the electromigration results obtained by controlled feedback in this material.

We should mention that due to the rather abrupt transition observed in the electromigration curve of Al, electropulsing in this material requires a very short dwell time and very well tuned voltage pulses. Attempts of achieving electropulsing in Al with few seconds scale pulses lead to immediate irreversible damage and the creation of nm scale gaps, similar to those reported in Ref. 16,22 for Au nanowires. Note that increasing the duration of the pulse allows to increase the local temperature at the electromigrated spot, which leads to an exponential change in the probability to induce damage, as sug-

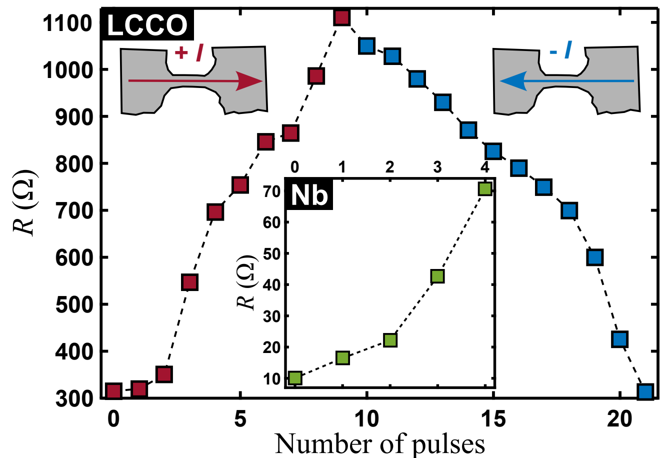

FIG. 6: **Electro-pulsing.** Main panel: values of resistance obtained after applying voltage pulses to a LCCO microbridge. Amplitude and duration of a single pulse were respectively 15 V and 1 s. Red points are taken after pulses of same polarity, blue points are taken after pulses of reversed polarity. Inset: same as in main panel but for Nb.

gested by Equation (1). On the other hand, increasing the amplitude of the voltage pulse increases the current density at the constriction which appears quadratically in Equation (1). We have succeeded in obtaining partial EM of Al constrictions by using pulses shorter than ms scale and by varying the amplitude of the pulse.

Conclusion

In conclusion, we investigated the benefits of controlled electromigration and its healing counterpart as a knob to adjust the normal state resistance of pre-indented superconducting nanoconstrictions down to fractions of Ohms. The forward electromigration works for the three investigated superconducting materials, whereas healing effects exhibit a material dependent performance. While EM in Al always leads to structural changes at the nanoconstriction, in Nb and $La_{2-x}Ce_xCuO_4$ there is a regime at low current densities where an irreversible response is observed but without associated structural damage. We attribute this effect to the selective electromigration of oxygen atoms. We also discuss the possibility to achieve rather efficient controlled electromigration by electropulsing, which can be straightforwardly implemented without investing efforts in costly analogue feedback systems or complex software controlled feedback loops. We highlight the appealing aspect of electromigration for investigating superconducting nanoconstrictions, with the possibility to beat the state-of-the-art lithography methods complemented by the reversibility of the process. We illustrate this fact by unveiling for the first time a current induced superconductor-to-insulator transition in $La_{2-x}Ce_xCuO_4$.

Experimental Section

Aluminum samples were patterned by electron beam lithography (EBL) on a Si/SiO_2 substrate (750 ± 50 μm Si, 300 ± 25 nm SiO_2) covered by a double layered PMMA resist mask, using a nanofabrication system from Raith GmbH. Subsequently, an Al thin film (∼25 nm) was deposited using molecular beam epitaxy (MBE) with a deposition rate of 1 Å/s and a pressure in the chamber under 10^{-8} mbar. The deposition was followed by a lift-off process. Scanning electron micrographs showing the sample layout with different magnifications are shown in Figure 1a-b. Figure 1c sketches the combined digital feedback loops used to carry out controlled electromigration. It consists of two algorithms working in parallel while ramping up the voltage: one intended to stabilize EM rate and another to prevent thermal runaways in case of fluctuations in the junction. In that context, $Th.$ represents the threshold rate defining thermal runaway, $f(\dot{G} - \dot{G}_S)$ the feedback function minimizing $|\dot{G} - \dot{G}_S|$, $\dot{G}_S$ the desired EM rate (set-point) and ΔV_{Th} the bias change needed to damp the thermal runaway.

The Nb samples with a thickness of 50 nm have been deposited by electron beam evaporation under a pressure of 10^{-8} mbar at a rate of 1.5 Å/s. On top of it, 5 nm of Si has been deposited for protecting the samples (pressure of $3 \cdot 10^{-9}$ mbar and rate of 0.5 Å/s). The lithographic electron exposure has been carried out in a Nanobeam nB5 platform with an electron beam energy of 80 keV. Afterwards, an aluminum mask was fabricated by e-beam evaporation, followed by a lift-off. To remove the Nb not covered by the aluminum, we performed reactive ion etching using SF_6 during 10 s. Finally, the aluminum was removed using the base developer MF-26A. Scanning electron micrographs showing the sample layout with different magnifications are shown in Figure 1d-e. The initial constriction width was about 130 nm, as indicated on Figure 1e.

The 100 nm thick high-T_c (LCCO) films were grown on (001)-oriented $SrTiO_3$ substrates by pulsed laser deposition, at temperatures ranging from 720 to 760 °C in an atmosphere of 0.13 mbar of pure oxygen. After the deposition, the films were annealed at the same temperature in vacuum for a few minutes to remove the excess of apical oxygen atoms, which are harmful to the superconductivity of electron-doped superconductors. The films were then slowly cooled down to room temperature in vacuum and finally patterned into microbridges by photolithography and Ar ion beam etching. Optical microscope images of the complete layout and the microconstriction are shown in Figure 1f and g, respectively. The white lines and dots observed in Figure 1g correspond to leftovers of the polymer resist mask and have no influence on the superconducting properties of the system. Figure 1h shows a magneto-optical image of a LCCO microbridge, evidencing a smooth penetration of magnetic flux into the sample. Dark areas correspond to low fields, while blue-white regions represent high fields. The homogeneity of the penetration is a strong indication of the high quality of the film, confirming excellent superconducting behaviour and absence of macroscopic defects. More information about the magneto-optical setup can be found in Ref. 53.

---

* Electronic address: xavier.baumans@ulg.ac.be

[1] P. B. Ghate, *Appl. Phys. Lett.* **1967**, *11*, 14–16.
[2] I. A. Blech, E. S. Meieran, *Appl. Phys. Lett.* **1967**, *11*, 263–266.
[3] R. Rosenberg, L. Berenbaum, *Appl. Phys. Lett.* **1968**, *12*, 201–204.
[4] J. R. Black, *Proceedings of the IEEE* **1969**, *57*, 1587–1594.
[5] F. d'Heurle, I. Ames, *Appl. Phys. Lett.* **1970**, *16*, 80–81.
[6] I. A. Blech, *J. Appl. Phys.* **1976**, *47*, 1203–1208.
[7] P. S. Ho, T. Kwok, *Rep. Prog. Phys.* **1989**, *52*, 301.
[8] M. F. Lambert, M. F. Goffman, J. P. Bourgoin, P. Hesto, *Nanotechnology* **2003**, *14*, 772.
[9] G. Esen, M. S. Fuhrer, *Appl. Phys. Lett.* **2005**, *87*, 263101.
[10] D. R. Strachan, D. E. Smith, D. E. Johnston, T.-H. Park, M. J. Therien, D. A. Bonnell, A. T. Johnson, *Appl. Phys. Lett.* **2005**, *86*, 043109.
[11] D. R. Strachan, D. E. Smith, M. D. Fischbein, D. E. Johnston, B. S. Guiton, M. Drndić, D. A. Bonnell, A. T. Johnson, *Nano Lett.* **2006**, *6*, 441–444.
[12] M. L. Trouwborst, S. J. v. d. Molen, B. J. v. Wees, *J. Appl. Phys.* **2006**, *99*, 114316.
[13] H. Park, J. Park, A. K. L. Lim, E. H. Anderson, A. P. Alivisatos, P. L. McEuen, *Nature* **2000**, *407*, 57–60.
[14] J. Park, A. N. Pasupathy, J. I. Goldsmith, C. Chang, Y. Yaish, J. R. Petta, M. Rinkoski, J. P. Sethna, H. D. Abrua, P. L. McEuen, D. C. Ralph, *Nature* **2002**, *417*, 722–725.
[15] L. H. Yu, D. Natelson, *Nano Lett.* **2004**, *4*, 79–83.
[16] N. Ittah, I. Yutsis, Y. Selzer, *Nano Lett.* **2008**, *8*, 3922–3927.
[17] J. M. Campbell, R. G. Knobel, *Appl. Phys. Lett.* **2013**, *102*, 023105.
[18] X. D. A. Baumans, D. Cerbu, O.-A. Adami, V. S. Zharinov, N. Verellen, G. Papari, J. E. Scheerder, G. Zhang, V. V. Moshchalkov, A. V. Silhanek, J. Van de Vondel, *Nat. Commun.* **2016**, *7*, 10560.
[19] W. Seith, S. Wever, *Z. Elektrochem.* **1953**, *57*, 891–900.
[20] T. Aref, A. Bezryadin, *Nanotechnology* **2011**, *22*, 395302.
[21] J. Moser, A. Barreiro, A. Bachtold, *Appl. Phys. Lett.* **2007**, *91*, 163513.
[22] C. Xiang, J. Y. Kim, R. M. Penner, *Nano Lett.* **2009**, *9*, 2133–2138.
[23] Z. Li, C. L. Bauer, S. Mahajan, A. G. Milnes, *J. Appl. Phys.* **1992**, *72*, 1821–1832.
[24] C.-F. Hong, M. Togo, K. Hoh, *Jpn. J. Appl. Phys.* **1993**, *32*, L624.
[25] T. Kozlova, M. Rudneva, H. W. Zandbergen, *Nanotechnology* **2013**, *24*, 505708.

[26] J. J. Spokas, C. P. Slichter, *Phys. Rev.* **1959**, *113*, 1462–1472.
[27] J. Bass, *Philo. Mag.* **1967**, *15*, 717–730.
[28] J. R. Lloyd, *Semicond. Sci. Technol.* **1997**, *12*, 1177.
[29] C.-Y. You, I. M. Sung, B.-K. Joe, *Appl. Phys. Lett.* **2006**, *89*, 222513.
[30] W. J. Skocpol, M. R. Beasley, M. Tinkham, *J. Appl. Phys.* **1974**, *45*, 4054–4066.
[31] K. Mizuno, T. Aomine, *J. Phys. Soc. Jpn.* **1980**, *48*, 1908–1913.
[32] H. Fangohr, D. S. Chernyshenko, M. Franchin, T. Fischbacher, G. Meier, *Phys. Rev. B* **2011**, *84*, 054437.
[33] W. Jeong, K. Kim, Y. Kim, W. Lee, P. Reddy, *Sci. Rep.* **2014**, *4*, 4975.
[34] V. S. Zharinov, *unpublished*.
[35] M. Zgirski, K. Y. Arutyunov, *Phys. Rev. B* **2007**, *75*, 172509.
[36] Y. Serruys, *Scr. Metall.* **1982**, *16*, 365–366.
[37] Y. Serruys, G. Brébec, *Philo. Mag. A* **1982**, *45*, 563–582.
[38] R. P. Gupta, Y. Serruys, G. Brébec, Y. Adda, *Phys. Rev. B* **1983**, *27*, 672–677.
[39] W. DeSorbo, *Phys. Rev.* **1963**, *132*, 107–121.
[40] J. Halbritter, *Appl. Phys. A* **1987**, *43*, 1–28.
[41] H. Shiraishi, K. Furuya, R. Watanabe, *J. Less Common Met.* **1979**, *63*, 147–158.
[42] M. Murakami, T. Yogi, *J. Appl. Phys.* **1985**, *57*, 211–215.
[43] A. K. Vijh, *J. Electrochem. Soc.* **1969**, *116*, 972–975.
[44] A. K. Vijh, *Oxid. Met.* **1972**, *4*, 63–71.
[45] K. G. Rajan, P. Parameswaran, J. Janaki, T. S. Radhakrishnan, *J. Phys. D: Appl. Phys.* **1990**, *23*, 694.
[46] B. H. Moeckly, R. A. Buhrman, *IEEE Trans. Appl. Supercond.* **1993**, *3*, 2038–2042.
[47] B. H. Moeckly, D. K. Lathrop, R. A. Buhrman, *Phys. Rev. B* **1993**, *47*, 400–417.
[48] B. H. Moeckly, R. A. Buhrman, P. E. Sulewski, *Appl. Phys. Lett.* **1994**, *64*, 1427–1429.
[49] R. F. Klie, J. P. Buban, M. Varela, A. Franceschetti, C. Jooss, Y. Zhu, N. D. Browning, S. T. Pantelides, S. J. Pennycook, *Nature* **2005**, *435*, 475–478.
[50] X. Zhang, H. Yu, G. He, W. Hu, J. Yuan, B. Zhu, K. Jin, *Phys. C* **2016**, *525-526*, 18–43.
[51] C. R. Rotundu, V. V. Struzhkin, M. S. Somayazulu, S. Sinogeikin, R. J. Hemley, R. L. Greene, *Phys. Rev. B* **2013**, *87*, 024506.
[52] P. Gao, Z. Kang, W. Fu, W. Wang, X. Bai, E. Wang, *J. Am. Chem. Soc.* **2010**, *132*, 4197–4201.
[53] J. Brisbois, O.-A. Adami, J. I. Avila, M. Motta, W. A. Ortiz, N. D. Nguyen, P. Vanderbemden, B. Vanderheyden, R. B. G. Kramer, A. V. Silhanek, *Phys. Rev. B* **2016**, *93*, 054521.